Polaron Photoconductivity in the Weak and Strong Light-Matter Coupling Regime

Nina Krainova,[1] Alex J. Grede,[1] Demetra Tsokkou,[2] Natalie Banerji,[2] and Noel C. Giebink[1,*]
[1]Department of Electrical Engineering, The Pennsylvania State University, University Park, Pennsylvania 16802, USA
[2]Department of Chemistry and Biochemistry, University of Bern, Bern, CH-3012, Switzerland

(Received 18 November 2019; accepted 14 April 2020; published 30 April 2020)

We investigate the potential for cavity-modified electron transfer in a doped organic semiconductor through the photocurrent that arises from exciting charged molecules (polarons). When the polaron optical transition is strongly coupled to a Fabry-Perot microcavity mode, we observe polaron polaritons in the photoconductivity action spectrum and find that their magnitude depends differently on applied electric field than photocurrent originating from the excitation of uncoupled polarons in the same cavity. Crucially, moving from positive to negative detuning causes the upper and lower polariton photocurrents to swap their field dependence, with the more polaronlike branch resembling that of an uncoupled excitation. These observations are understood on the basis of a phenomenological model in which strong coupling alters the Onsager dissociation of polarons from their dopant counterions by effectively increasing the thermalization length of the photoexcited charge carrier.

DOI: 10.1103/PhysRevLett.124.177401

The notion that optical environment can change the nature of a chemical reaction emerges in the strong coupling regime when molecular electronic (or vibrational) transitions hybridize with light to form polariton states that have different energies, coherence, and dynamical characteristics than the bare (uncoupled) molecules themselves [1–5]. Dubbed polariton chemistry [6,7], a growing body of work has now established that it is indeed possible to alter the rate or yield of certain photochemical reactions [1,8,9] (and possibly some reactions in the dark [10–12]) by strong coupling the participant molecules to an optical microcavity or plasmon mode.

Photoinduced charge transfer is arguably one of the most important areas to explore such modification since it underlies processes ranging from photolithography to photosynthesis. In this case, strong coupling is predicted to alter both the free energy driving force of the reaction (dependent on the polariton energy) and its reorganization energy due to polaron decoupling (where polaritons preserve the ground state nuclear configuration) [4]. Whether measurable changes in electron transfer rate can be observed in practice is, however, an open question since any such changes must compete with the extremely short (< 100 fs) polariton lifetime [13] in typical metal microcavity and plasmon systems. Moreover, given that the optical properties of polaritons in most organic materials are well described classically based on their natural dielectric function, it is reasonable to ask whether chemically distinct polariton states truly emerge.

Here, we explore these questions by measuring the photoconductivity of a *p*-doped organic semiconductor in which charged, rather than neutral molecules (i.e., polaronic rather than excitonic states), are strongly coupled to a Fabry-Perot microcavity. We confirm the existence of polaron polariton modes in the photoconductivity action spectrum and find that their magnitude evolves differently with applied bias than photocurrent that originates from exciting uncoupled polarons in the same cavity. Importantly, the difference in functional dependence changes systematically with the polariton detuning, leading us to conclude that these observations reflect a genuine change in the underlying photoinduced electron transfer process that occurs following the excitation of each species.

As in previous work [14], we study the organic semiconductor 4,4'-cyclohexylidenebis[*N*,*N*-bis(4-methylphenyl)benzenamine] (TAPC) doped with MoO_3. The high electron affinity of MoO_3 induces ground state electron transfer from the highest occupied molecular orbital (HOMO) of TAPC, yielding a large density of holes (i.e., TAPC cations) that absorb strongly with a peak at $\sim$1.8 eV and shoulder at $\sim$2.1 eV [Fig. 1(a)] due to excitation of the hole downward into lower-lying molecular orbitals [14]. The same transitions are observed in the photocurrent external quantum efficiency (EQE) spectrum shown in Fig. 1(a) for a sandwich-type device consisting of indium-tin-oxide (140 nm)/30 vol% MoO_3:TAPC (160 nm)/Ag (20 nm) as illustrated in the inset. There, the magnitude of the EQE spectrum (measured under chopped illumination using lock-in detection) increases with bias and its shape remains constant, independent of the bias polarity. The dashed lines in Fig. 1(b) show the component peaks that make up the polaron EQE spectrum superimposed on an exponential background thought to be associated with photocurrent generation from the absorption tail of neutral TAPC [15] (i.e., due to exciton dissociation). Note that the photocurrent measurements

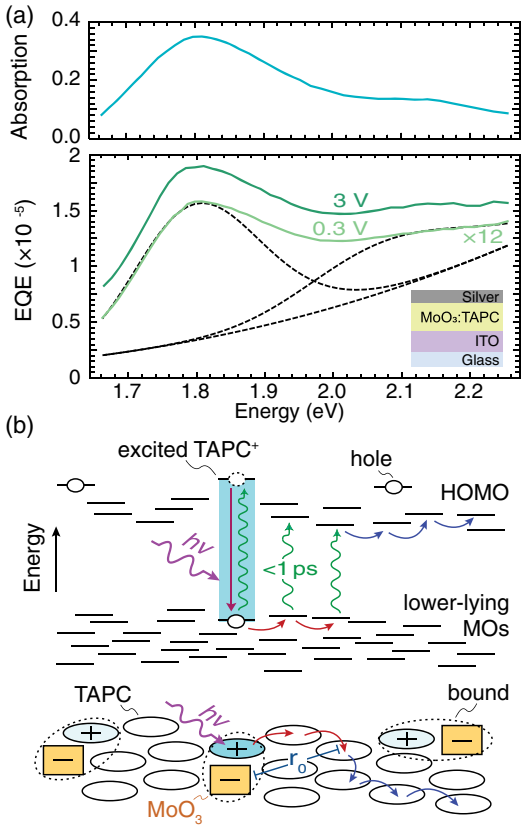

FIG. 1. (a) Photocurrent EQE spectra measured at $T = 100$ K for a 160-nm-thick, 30% MoO_3:TAPC film using the sandwich-type device structure shown in the inset. The shape of the EQE spectrum remains constant from low (0.3 V) to high (3 V) bias and consists of two peaks (the dashed lines are the result of a multipeak fit) that correspond with those observed in the polaron optical absorption spectrum of the bare film (measured at $T = 100$ K, accounting for transmission and reflection) shown in the top panel. (b) Schematic of the polaron photoconductivity mechanism in energy (top) and real space (bottom).

are conducted at low temperature to minimize the background dark current flowing in the highly doped film (its conductivity is thermally activated) [16,17]. The EQE data at room temperature are qualitatively similar, except the polaron features are slightly broader and the overall magnitude of the spectra is roughly 2 orders of magnitude higher.

Polaron photoconductivity of this sort has not previously been studied in organic semiconductors but is probably analogous to that in traditional inorganic photoconductors such as Hg-doped Ge [18], where photon absorption liberates a trapped hole from a shallow acceptor dopant [Fig. 1(b)]. In the case of MoO_3-doped TAPC, the vast majority of holes at room temperature and below are trapped in the weakly screened Coulomb potential of the MoO_3 counterions [16,17]. This is evident from the fact that the hole concentration inferred from electrical conductivity measurements ($\lesssim 10^{18}$ cm^{-3}) [19] is typically orders of magnitude lower than that inferred from the polaron absorption coefficient ($\sim 10^{20}$ cm^{-3})[15], particularly at low temperature [16]. Thus, the majority of polaron absorption is due to bound rather than free holes. Exciting a bound hole to a lower-lying molecular orbital can liberate it through one or more hops (i.e., electron transfer events) in the excited state, as illustrated by the red arrows in Fig. 1(b). However, because excited state hopping competes with ultrafast relaxation back to the HOMO (<1 ps based on transient absorption measurements shown in the Supplemental Material [20], which includes Ref. [21]), only one or two such excited state hops can realistically occur, leaving the relaxed hole only slightly farther from its counterion than where it started. The resulting picture is then very similar to a traditional Onsager-type dissociation process [22,23], with drift and diffusive escape from the counterion Coulomb potential beginning from an initial "thermalization" distance r_0, as indicated by the blue arrows in Fig. 1(b).

Photocurrent in the strong coupling regime is subsequently explored by replacing the indium-tin-oxide contact with an optically thick 100 nm Al mirror and maintaining the MoO_3:TAPC layer thickness at $d = 160$ nm to achieve a zero-detuned microcavity with respect to the peak of the main polaron transition. Strong coupling is verified by angle-dependent reflectivity measurements shown in the Supplemental Material [20], which yield upper and lower polariton (UP and LP, respectively) modes with a vacuum Rabi splitting of $\hbar\Omega \approx 0.25$ eV.

Figures 2(a) and 2(b), respectively, show the magnitude and phase (φ) of the photocurrent spectrum measured for this sample at an incident angle of $\theta = 0°$, close to the anticrossing point in the dispersion. In contrast to the weakly coupled case in Fig. 1, the shape of the spectra in Fig. 2(a) changes dramatically with bias, evolving from a single peak near the bare polaron energy at low bias to a double peak reminiscent of the polariton modes at high bias. Similarly, the phase of the photocurrent in Fig. 2(b) exhibits a strong spectral variation at low bias that differs from the spectrally flat, simple sign flip (i.e., φ changes from 0° to 180° upon reversing the bias polarity) that occurs in the weakly coupled control case.

At this stage, it is important to bear in mind that the photocurrent is, in general, composed of both drift and diffusion components, and that the diffusion contribution due, e.g., to the large optical intensity gradient in the cavity, might become dominant at low bias since drift is proportional to the applied electric field. Without knowing the details of either component, it is nevertheless possible to separate them by recognizing that the drift component reverses direction upon changing the bias polarity (there is no built-in potential in the device as inferred from its symmetric current-voltage characteristic shown in the Supplemental Material [20], which includes Refs. [24–28]), whereas the diffusion current does not. Thus, adding the photocurrent phasors at a given positive and negative

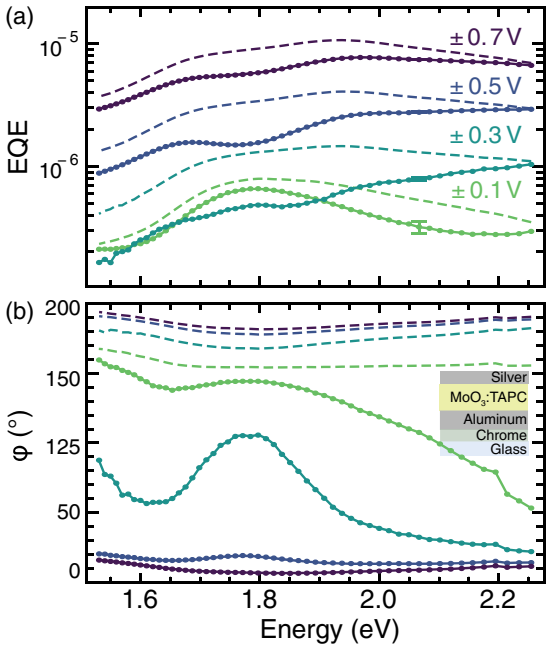

FIG. 2. (a) EQE magnitude spectra obtained from the microcavity shown in inset of (b) at varying negative (dashed) and positive (symbols) biases. Light is normally incident on the cavity and the data are collected at a temperature of 100 K. (b) Corresponding phase of the photocurrent relative to the chopper reference signal at 389 Hz. The device structure is shown in the inset.

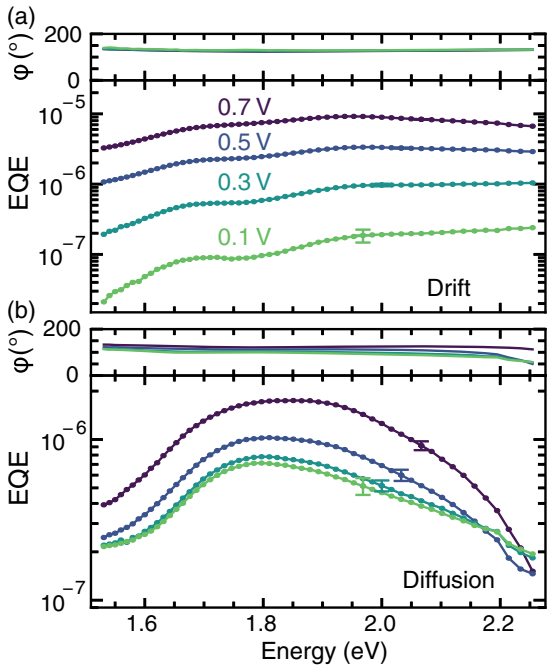

FIG. 3. (a) Drift and (b) diffusion photocurrent spectra obtained by decomposing the raw data in Fig. 2 as described in the text. The bottom portion of the plot in each panel shows the magnitude and the top portion shows the phase.

bias eliminates the drift, yielding twice the diffusion, and subtracting them yields twice the drift, as illustrated in the Supplemental Material [20].

The resulting drift- and diffusion-only photocurrents are plotted in Figs. 3(a) and 3(b), respectively. The validity of this separation procedure follows from the fact that it collapses the complicated dataset in Fig. 2 to a single bias-independent diffusion current spectrum in Fig. 3(b), while also obtaining constant phase spectra for both drift and diffusion (shown at the top of each plot), as expected since the dynamics of the dissociation process are orders of magnitude faster than the chopping frequency. The apparent increase in diffusion current magnitude at high biases is likely an artifact associated with the difficulty inherent in attempting to extract a small difference from two large numbers (i.e., the drift contribution dominates at high bias).

In Fig. 3(a), the overall magnitude of the drift current increases with bias as expected; however, there is also a subtle change in the spectrum: the polariton peaks become less prominent due to an increase in the EQE in the region between them at high bias. This is more clearly evident in Fig. 4, which plots the low- and high-bias drift spectra (bottom and top plots, respectively) normalized on a linear scale for incidence angles of $\theta = 0°$ and $\theta = 60°$. Crucially, the device reflectivity is *independent* of bias and thus these data imply that the field dependence of the photogeneration process changes depending on the angle of excitation.

The dashed lines in Fig. 4 represent the components of a phenomenological multipeak fit, where the green and cyan curves are fixed at the uncoupled polaron transition energies from Fig. 1(a) and the red and blue "polariton" peaks are varied to best fit the data; the dispersion of the latter is shown together with that from reflectivity in the Supplemental Material [20]. Evidently, the spectral evolution at $\theta = 0°$ near the anticrossing point can be understood as a growing contribution from uncoupled polaron photoconductivity as the bias increases. No such contribution is required to describe the evolution at positive detuning ($\theta = 60°$), which may simply reflect the fact that the data do not constrain separate peaks in the fit when the LP is so close to the uncoupled transition.

Figure 5 summarizes the bias dependence of the UP, LP, and uncoupled polaron component amplitudes from Figs. 4(a) and 4(b) along with those from the intermediate angle of $\theta = 45°$ and data from two additional cavities with different thicknesses ($d = 125$ and $d = 190$ nm) to cover a wider range of detuning; the fitting analysis of these cavities is provided in the Supplemental Material [20]. Two important observations follow from these data. First, the uncoupled polaron contribution only emerges at low bias near zero detuning and exhibits a stronger field dependence than the polariton modes. Second, the nearly identical field dependence of the UP and LP contributions at zero detuning gives way to a deviation at low bias in the positive and negative detuning regimes, with the more polaronlike branch exhibiting a stronger field dependence.

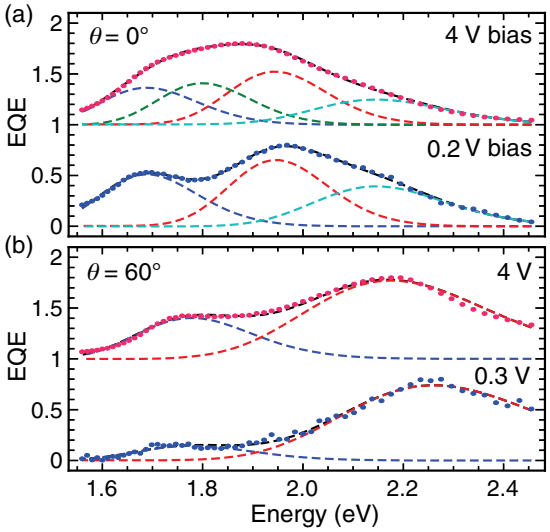

FIG. 4. (a) Comparison of the drift magnitude spectra obtained from Fig. 3(a) at low and high bias. The spectra are normalized and offset for clarity. Dashed lines result from Gaussian multipeak fitting of the spectra, where the red, blue, green, and cyan lines nominally correspond to the UP, LP, and uncoupled polaron main and shoulder transitions identified in Fig. 1(a). (b) Analogous results obtained from the same cavity at 60° incidence angle. No contribution from the uncoupled polaron can be discerned in the fit.

We emphasize that there is no spectral variation in the bias dependence of the weakly coupled device, as evident from the unchanging EQE line shape in Fig. 1(a) and shown explicitly in the Supplemental Material [20].

The most likely means by which strong coupling might affect the field dependence of photoconductivity is by influencing the initial dissociation of an excited TAPC hole from its MoO_3 counterion, since subsequent conduction through the device should not depend on how the hole is

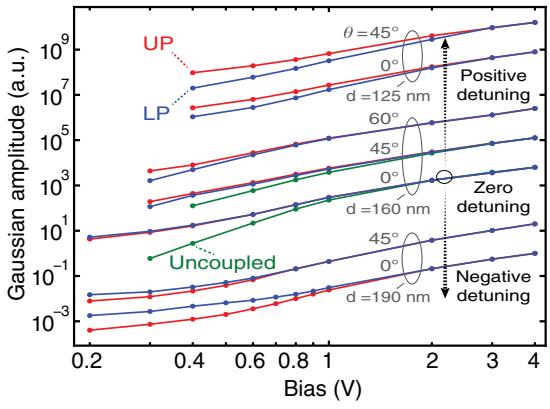

FIG. 5. Bias dependence of the UP (red), LP (blue), and uncoupled polaron (green) peak amplitudes fit from the data in Fig. 4, along with analogous datasets obtained for two additional cavities with different thicknesses as indicated in the plot. Each dataset is normalized at 4 V and vertically offset for clarity. The uncoupled polaron contribution can only be reliably discerned in the spectra near zero detuning.

generated (thermal, optical, etc.). Given that the dependence of the dissociation yield η on electric field F is strongly influenced by the thermalization length in Onsager theory (where larger r_0 leads to a weaker field dependence; see the Supplemental Material [20], which includes Refs. [27–32]), one interpretation of the deviation between the polariton and uncoupled polaron slopes in Fig. 5 is that strong coupling effectively increases r_0.

At a mechanistic level, such a change would presumably reflect a difference in the electron transfer rate (i.e., associated with movement of the excited hole) from a delocalized polaritonic $TAPC^+$ excitation to neighboring TAPC molecules as compared to that originating from an uncoupled (i.e., localized) $TAPC^+$ excitation. Importantly, because electron transfer from a polariton state should, in general, destroy its coherence (due to the low probability of the acceptor molecule being one of the few that are coherently coupled in a given polaritonic excitation), only the first electron transfer event in the chain from Fig. 1(b) might be altered. Moreover, since the electron transfer rate associated with hole hopping ($k_{et} < 1$ ps^{-1}) is generally slow compared with the polariton decay rate ($\sim$100 ps^{-1} corresponding to a lifetime of $\tau \sim 10$ fs), only a small number of such events could actually be modified in the first place. This difference in timescale explains why no change in reflectivity is observed, since polariton decay is essentially unaffected by changes in electron transfer rate.

The picture that emerges is thus one in which most polaritonic excitations decay and dephase naturally into incoherent excited states that contribute to photoconductivity in the same manner as in the weakly coupled device. A small fraction ($\phi_{et} \sim k_{et}\tau$) of the polaritons decay via charge transfer, yielding a larger thermalization length on average and thus more facile dissociation at low field. Uncoupled polarons are excited with finite probability near zero detuning due to the imperfect cavity, resulting in a photoconductivity contribution that falls off more sharply with applied field due to their smaller thermalization length. At positive or negative detuning, the field dependence of the more polaronlike branch begins to resemble that of the uncoupled excitation. A simple Onsager photoconductivity model based on these considerations can reproduce the difference in field dependence that emerges between the polariton and uncoupled photocurrent contributions at low bias, as shown in the Supplemental Material [20].

The origin of the polariton-enhanced charge transfer that we infer from these results is not yet clear. It could be due to the polaron decoupling mechanism proposed in Ref. [4]; however, the near-identical UP and LP field dependence that we observe at zero detuning is difficult to reconcile with this theory and the Rabi splitting in our devices is probably too small for significant polaron decoupling effects to begin with. An alternative explanation might stem from the disordered nature of the system and the

natural variation in intermolecular electronic coupling that exists between pairs of molecules with different orientations, separations, and conformations. In the case of a localized excitation, electron transfer is governed by the electronic coupling of that molecule with its neighbors. A polaritonic excitation on the other hand, is delocalized over many molecules and therefore can effectively sample many more electronic couplings, potentially benefiting from the largest in the subensemble to speed up the overall charge transfer rate. A simple rate model captures the essence of this mechanism in the Supplemental Material [20], which includes Refs. [33,34].

In summary, we have found that the photoconductivity of TAPC hole polarons systematically changes when they are strongly coupled to a microcavity mode in a manner that is consistent with polaritonic modification of the initial photo-induced electron transfer event involved in dissociating Coulombically bound holes from their MoO_3 counterions. In principle, the same phenomenon should also occur for neutral exciton-polaritons since exciton dissociation is a similar process, though we emphasize that a low dissociation yield is key given that subtle changes in dissociation dynamics have little effect on yield if the process is already efficient (e.g., as in the case of strongly coupled donor-acceptor systems [35]). This similarity, combined with the convenience of using photocurrent to infer changes in electron transfer, should make both strongly coupled exciton and polaron systems fertile ground for testing theoretical developments in cavity controlled electron transfer in the future.

We thank S. Kéna-Cohen and J. Yuen-Zhou for helpful discussions. This work was supported in part by the Charles E. Kaufman Foundation, DARPA Grant No. D19AC00011, and NSF Grant No. DMR-1654077. N. B. and D. T. thank the European Research Council (ERC) for supporting this research by a Starting Grant (No. 714586, OSIRIS) as well as the University of Bern for funding. N. B. thanks the Swiss National Science foundation (Grant No. 200020_184819).

*ncg2@psu.edu

[1] J. A. Hutchison, T. Schwartz, C. Genet, E. Devaux, and T. W. Ebbesen, Angew. Chem. Int. Ed. **51**, 1592 (2012).
[2] F. C. Spano, J. Chem. Phys. **142**, 184707 (2015).
[3] J. Galego, F. J. Garcia-Vidal, and J. Feist, Nat. Commun. **7**, 13841 (2016).
[4] F. Herrera and F. C. Spano, Phys. Rev. Lett. **116**, 238301 (2016).
[5] C. Schafer, M. Ruggenthaler, H. Appel, and A. Rubio, Proc. Natl. Acad. Sci. U.S.A. **116**, 4883 (2019).
[6] R. F. Ribeiro, L. A. Martínez-Martínez, M. Du, J. Campos-Gonzalez-Angulo, and J. Yuen-Zhou, Chem. Sci. **9**, 6325 (2018).
[7] J. Feist, J. Galego, and F. J. Garcia-Vidal, ACS Photonics **5**, 205 (2018).
[8] B. Munkhbat, M. Wersäll, D. G. Baranov, T. J. Antosiewicz, and T. Shegai, Sci. Adv. **4**, eaas9552 (2018).
[9] K. Stranius, M. Hertzog, and K. Borjesson, Nat. Commun. **9**, 2273 (2018).
[10] E. Orgiu, J. George, J. A. Hutchison, E. Devaux, J. F. Dayen, B. Doudin, F. Stellacci, C. Genet, J. Schachenmayer, C. Genes, G. Pupillo, P. Samorì, and T. W. Ebbesen, Nat. Mater. **14**, 1123 (2015).
[11] A. Thomas, J. George, A. Shalabney, M. Dryzhakov, S. J. Varma, J. Moran, T. Chervy, X. Zhong, E. Devaux, C. Genet, J. A. Hutchison, and T. W. Ebbesen, Angew. Chem. Int. Ed. **55**, 11462 (2016).
[12] A. Thomas, L. Lethuillier-Karl, K. Nagarajan, R. M. A. Vergauwe, J. George, T. Chervy, A. Shalabney, E. Devaux, C. Genet, J. Moran, and T. W. Ebbesen, Science **363**, 615 (2019).
[13] D. G. Lidzey, A. M. Fox, M. D. Rahn, M. S. Skolnick, V. M. Agranovich, and S. Walker, Phys. Rev. B **65**, 195312 (2002).
[14] C.-Y. Cheng, R. Dhanker, C. L. Gray, S. Mukhopadhyay, E. R. Kennehan, J. B. Asbury, A. Sokolov, and N. C. Giebink, Phys. Rev. Lett. **120**, 017402 (2018).
[15] C.-Y. Cheng, H. Kim, and N. C. Giebink, ACS Photonics **6**, 308 (2019).
[16] M. L. Tietze, J. Benduhn, P. Pahner, B. Nell, M. Schwarze, H. Kleemann, M. Krammer, K. Zojer, K. Vandewal, and K. Leo, Nat. Commun. **9**, 1182 (2018).
[17] M. Schwarze, C. Gaul, R. Scholz, F. Bussolotti, A. Hofacker, K. S. Schellhammer, B. Nell, B. D. Naab, Z. Bao, D. Spoltore, K. Vandewal, J. Widmer, S. Kera, N. Ueno, F. Ortmann, and K. Leo, Nat. Mater. **18**, 242 (2019).
[18] N. Sclar, Prog. Quantum Electron. **9**, 149 (1984).
[19] M. Kröger, S. Hamwi, J. Meyer, T. Riedl, W. Kowalsky, and A. Kahn, Org. Electron. **10**, 932 (2009).
[20] See Supplemental Material at http://link.aps.org/supplemental/10.1103/PhysRevLett.124.177401 for experimental methods, supporting data, and a model of the polariton photocurrent.
[21] M. Fujitsuka and T. Majima, J. Photochem. Photobiol. C Photochem. Rev. **35**, 25 (2018).
[22] L. Onsager, Phys. Rev. **54**, 554 (1938).
[23] M. Pope and C. E. Swenberg, *Electronic Processes in Organic Crystals and Polymers* (Oxford University Press, New York, 1999).
[24] J. G. Simmons, J. Appl. Phys. **34**, 1793 (1963).
[25] J. G. Simmons, J. Appl. Phys. **35**, 2655 (1964).
[26] E. J. Patio and N. G. Kelkar, Appl. Phys. Lett. **107**, 253502 (2015).
[27] V. I. Arkhipov, P. Heremans, E. V. Emelianova, and H. Bässler, Phys. Rev. B **71**, 045214 (2005).
[28] V. I. Arkhipov, E. V. Emelianova, P. Heremans, and H. Bässler, Phys. Rev. B **72**, 235202 (2005).
[29] D. Hertel and H. Bässler, Chem. Phys. Chem. **9**, 666 (2008).
[30] P. M. Borsenberger and A. I. Ateya, J. Appl. Phys. **49**, 4035 (1978).
[31] D. M. Pai and R. C. Enck, Phys. Rev. B **11**, 5163 (1975).
[32] A. Mozumder, J. Chem. Phys. **60**, 4300 (1974).
[33] H. Bassler, Phys. Status Solidi (b) **175**, 15 (1993).
[34] P. M. Borsenberger, E. H. Magin, M. D. Van Auweraer, and F. C. De Schryver, Phys. Status Solidi (a) **140**, 9 (1993).
[35] E. Eizner, J. Brodeur, F. Barachati, A. Sridharan, and S. Kena-Cohen, ACS Photonics **5**, 2921 (2018).